catalysts

MDPI

Article

Effects of Operating Parameters and Feed Gas Compositions on the Dry Reforming of Methane over the Ni/Al_2O_3 Catalyst

Eunju Yoo, Dong-Seop Choi, Jiyull Kim, Yoon-Hee Kim, Na-Yeon Kim and Ji Bong Joo *

Department of Chemical Engineering, Konkuk University, 120 Neungdong-ro, Gwangjin-gu, Seoul 05029, Republic of Korea; kny960403@konkuk.ac.kr (N.-Y.K.)
* Correspondence: jbjoo@konkuk.ac.kr; Tel.: +82-2-450-3545

Abstract: The effects of operating parameters such as reaction temperature, space velocity, and feed gas composition on the performance of the methane dry-reforming reaction (DRM) over the Ni/Al_2O_3 catalyst are systemically investigated. The Ni/Al_2O_3 catalyst, which is synthesized by conventional wet impregnation, showed well-developed mesoporosity with well-dispersed Ni nanoparticles. CH_4 and CO_2 conversions over the Ni/Al_2O_3 catalyst are dramatically increased as both the reaction temperature is increased, and space velocity is decreased. The feed gas composition, especially the CO_2/CH_4 ratio, significantly influences the DRM performance, catalyst deactivation and the reaction behavior of side reactions. When the CO_2-rich gas composition ($CO_2/CH_4 > 1$) was used, a reverse water gas shift (RWGS) reaction significantly occurred, leading to the consumption of hydrogen produced from DRM. The CH_4-rich gas composition ($CO_2/CH_4 < 1$) induces severe carbon depositions followed by a reverse Boudouard reaction, resulting in catalytic activity drastically decreasing at the beginning followed by a stable conversion. The catalyst after the DRM reaction with a different feed ratio was analyzed to investigate the amount and structure of carbon deposited on the catalyst. In this study, we suggested that the optimal DRM reaction conditions can achieve stable performances in terms of conversion, hydrogen production and long-term stability.

Keywords: dry reforming; operation parameter; carbon deposition

Citation: Yoo, E.; Choi, D.-S.; Kim, J.; Kim, Y.-H.; Kim, N.-Y.; Joo, J.B. Effects of Operating Parameters and Feed Gas Compositions on the Dry Reforming of Methane over the Ni/Al_2O_3 Catalyst. *Catalysts* **2023**, *13*, 602. https://doi.org/10.3390/catal13030602

Academic Editors: Kee Young Koo and Unho Jung

Received: 4 January 2023
Revised: 13 March 2023
Accepted: 14 March 2023
Published: 16 March 2023

1. Introduction

Industrial development provided mankind with a great deal of convenience. As the industrialized civilization continues to develop, our society has relied heavily on fossil-fuel-based energy resources. Most industrial advancements have been accompanied by fossil fuel use. However, technological improvements based on the use of fossil fuel have contributed to increasing greenhouse gas emissions [1]. Climate change, which causes a rise in sea level, heat waves and desertification, is largely accepted as a result of greenhouse gas emissions from the use of fossil fuel energy [2].

To mitigate global climate change caused by greenhouse gases, sustainable and eco-friendly energy systems should be explored and implanted to replace fossil-fuel-based energy [3]. Biogas, composed mainly of methane and carbon dioxide, can be produced by the anaerobic digestion of organic wastes such as sewage sludge, food waste, and livestock night soil [4–6]. This gas can be used to generate heat and power generation and can be purified and upgraded to biomethane for further energy applications [7,8]. In addition, biomethane can be converted to syngas (CO/H_2) through catalytic reforming processes and CO_2 separation processes such as steam methane reforming (SMR) and pressure swing adsorption (PSA) [9].

It is well known that the CH_4-to-CO_2 ratio in biogas is generally in the range from 7:3 to 5.5:4.5, which is highly dependent on the feedstock of biogas generation [10]. The methane content in landfill gas (LFG) is about 40–60%, while the methane content of the gas generated by the anaerobic digestion of sewage sludge is about 40–50% On the other

hand, the methane content in the biogas produced by the livestock manure of food waste treatment is 50–70%, which is relatively high [11]. Furthermore, the methane-rich biogas can directly be converted to produce syngas (CO/H_2) and green hydrogen through the dry-reforming reaction of methane (DRM) with a small makeup of CO_2 followed by a water shift reaction (WGS) [12]. Since CH_4 and CO_2 in purified biogas can be directly utilized without any expensive PSA separation units, there has been increased attention recently focused on biogas-linked DRM reactions for green hydrogen production [13].

It is widely acknowledged that the dry reforming of methane (DRM) is an effective method for producing syngas from methane and carbon dioxide—two greenhouse gases—without additional carbon dioxide emissions [14]. Additionally, syngas can be converted into valuable chemicals and used for hydrogen production [15]. When biogas —which has highly variable methane content—is applied directly to the DRM process, the H_2/CO ratio of the resultant syngas can be adjusted. However, this can lead to an increased tendency for carbon deposition [16]. Therefore, it is necessary to evaluate how catalytic activity is affected when the feed composition is changed, as well as which operation parameters are essential for reaction performance. To maximize efficiency, the DRM reaction unit and catalysts must be tailored to the target biogas stream.

Although numerous catalysts have been suggested in fundamental research, Ni-based catalysts are commonly used in both lab-scale and practical processes in the methane reformation processes due to high catalytic activity, relatively low cost and wide availability [17–19]. Generally, it is accepted that Ni-based catalysts are the most effective ones on reforming reactions. So far, most studies on reforming catalysts are mainly focused on $Ni\text{-}Al_2O_3$-based catalysts and the one for DRM reaction is no exception [19,20]. The dry-reforming process, which is a highly endothermic reaction (Equation (1)), is usually carried out at high reaction temperatures (700–850 °C). These high-temperature conditions often induce the agglomeration of nickel particles (also known as thermal sintering), leading to the loss of the number of active sites and deactivation of the catalyst [21,22]. In addition, the aggregated Ni particles can accelerate the formation of carbon (coking), resulting in an overall performance drop of the DRM unit [23].

$$CH_4 + CO_2 \rightarrow 2H_2 + 2CO \cdots \Delta H_{298K} = 247\ kJ{\cdot}mol^{-1} \quad (1)$$

Many researchers have sought to understand the relationships between the catalytic chemistry of Ni-based catalysts and reaction conditions in methane dry-reforming environments. Song et al. proposed a locking mechanism wherein the suitable particle size of active metal remains a crucial factor in achieving sintering resistance, even after extended testing. They demonstrated that metal particulates move on high-energy step edges of the support during activation to form stable particles. In addition, they exhibited that carbon deposition (coking) easily occurs on Ni catalysts when operating a dry-reforming reaction at low temperatures [24]. Charisiou et al. reported that carbon deposition and defects in the carbon increased as the reaction temperature decreased from 800 to 600 °C [25]. Research groups have studied catalyst deactivation by varying reaction temperatures to understand the activity and durability of Ni-based catalysts [17,26]. However, there is not enough research that comprehensively compares the effect of operating parameters in the dry-reforming process, focusing on the feed gas composition and side reactions. It is still difficult to systematically investigate the catalytic activity, coke formation and reaction behavior according to operating conditions such as temperature, WHSV and gas compositions for the syngas–hydrogen production via practical biogas-linked DRM reactors. The optimal conditions for maximizing syngas yield and minimizing coking must be also figured out, since purified biogas can intrinsically contain CH_4-rich gas. Furthermore, it is critical to identify the optimal operating conditions of the dry-reforming reaction on each situational case for designing practical biogas-linked DRM processes which can be applied to practical organic waste treatment sites. This is because the composition of feed biogas can be varied. By controlling the operating parameters, it is possible to reduce carbon deposition and increase hydrogen yield while suppressing undesirable side reactions.

In this study, we synthesized a conventional Ni/Al_2O_3 catalyst which is well known as a highly active catalyst in methane conversion reactions. The characteristics of the catalyst were investigated by BET, XRD, TEM and H_2-TPR. We applied the catalyst to the dry-reforming reaction of CO_2/CH_4 using the model purified-biogas stream. We investigated the effects of operating conditions such as temperature, WHSV and the CO_2-to-CH_4 ratio on the DRM reaction, and both the reaction activity and deactivation behavior of the Ni/Al_2O_3 catalyst are systemically studied. In addition, we also investigated the relationship between operation conditions and the tendency of side reactions. The spent catalyst with a different feed ratio was also analyzed with TGA, TEM and Raman spectroscopy. In this paper, we discussed our systemically experimental results and suggested the optimal operation window of the DRM unit which could be potentially used for designing practical biogas-linked DRM processes.

2. Results and Discussion

Figure 1 shows the physical and chemical properties of alumina support and Ni/Al_2O_3 catalysts. Figure 1a illustrates the N_2 adsorption–desorption isotherms and the corresponding pore size distribution of the mother Al_2O_3 support and the calcined Ni/Al_2O_3 catalyst. The commercial alumina support exhibited a type-IV isotherm, which is associated with capillary condensation in mesopores [27]. It exhibited precipitous adsorption at the relative pressure of approximately 0.7–0.8, suggesting that the original Al_2O_3 sample had a considerably uniform mesopore with well-developed pore connectivity [28]. Furthermore, Ni/Al_2O_3 showed a similar isotherm pattern, although its adsorbed volume was slightly lower than the original Al_2O_3 support. This suggests that the mesoporous structure of the Al_2O_3 support is well preserved even after Ni loading and calcination. This is further confirmed by the results of the pore size distribution (PSD) (see Figure 1a inset). Both Al_2O_3 support and Ni/Al_2O_3 catalysts have similar PSD patterns which show a sharp distribution peak in the range of 5–10 nm with the maximum point at ca. 7.4 nm. The calculated surface area and pore volumes of Ni/Al_2O_3 catalyst (153.7 m^2/g and 0.38 cm^3/g) are slightly smaller than those of original Al_2O_3 support (213.9 m^2/g and 0.52 cm^3/g), respectively. This indicates that some nickel oxide nanoparticles may have grown inside the pore during the nickel impregnation that followed the calcination step, which results in the pore blockage of alumina support.

Figure 1b presents X-ray diffraction (XRD) patterns of the alumina support, calcined Ni/Al_2O_3 catalyst and the Ni/Al_2O_3 catalyst after reduction at 800 °C. The alumina support exhibits clear peaks at 2θ = 37.8, 45.7 and 66.8°, indicating a typical γ-Al_2O_3 (ICDD PDF 00-029-0063) phase. The peaks related to the γ-Al_2O_3 phase are well maintained even after Ni loading, followed by calcination and reduction in all samples. After calcination, the Ni/Al_2O_3 catalyst shows an increment of peak intensity around 2θ = 37°, which indicates the existence of the $NiAl_2O_4$ (ICDD PDF 00-010-0339) phase. The calcined Ni/Al_2O_3 catalyst had a weak shoulder peak at 2θ = 43°, which indicates the presence of NiO (ICDD PDF 00-044-1159) nanoparticles highly dispersed on the support. For the reduced Ni/Al_2O_3 catalyst, the peak related to NiO disappeared and new diffraction peaks appeared. The reduced Ni/Al_2O_3 showed obvious diffraction peaks at 44.3, 51.7 and 76.2° which ascribe to (111), (200) and (220) planes of metallic Ni. The average crystallite size of the Ni nanoparticle of the reduced Ni/Al_2O_3 was estimated using the Scherrer equation based on the (200) peak and was found to be approximately 11 nm.

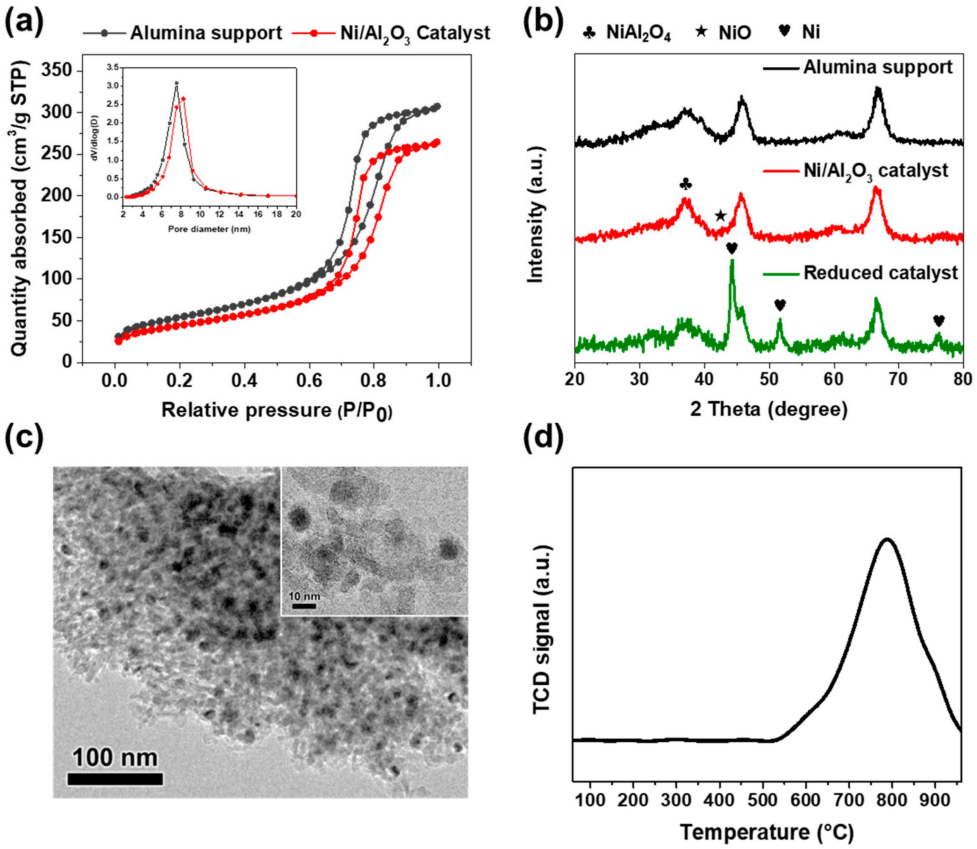

Figure 1. (**a**) N_2 adsorption–desorption isotherms and pore diameter distribution of alumina support and Ni/Al_2O_3 catalyst, (**b**) X-ray diffraction (XRD) patterns of alumina support, Ni/Al_2O_3 catalyst, and reduced Ni/Al_2O_3 catalyst, (**c**) Transmission Electron Microscopy (TEM) images of reduced Ni/Al_2O_3 catalyst, and (**d**) H_2 temperature-programmed reduction (H_2-TPR) profile of Ni/Al_2O_3 catalyst from 60 to 960 °C with a linear rate of 5 °C/min.

We investigated the overall morphology and metal dispersion of the reduced Ni/Al_2O_3 catalyst by TEM analysis. As shown in Figure 1c, it can be easily observed that alumina support has a porous structure, and the nickel nanoparticles are well dispersed both on the surface and inside the pore of alumina support. The observed size of the supported Ni nanoparticles was ca. 11 nm. This is consistent with the results of the XRD analysis.

The hydrogen temperature-programmed reduction (H_2-TPR) was conducted to examine the reduction characteristics of the Ni/Al_2O_3 catalyst (Figure 1d). As shown in the TPR results, the reduction starts at ca. 520 °C, and then the maximum peak is observed at ca. 786 °C. The hydrogen is continuously consumed until 970 °C. The Ni/Al_2O_3 catalyst exhibits different reduction patterns according to the interaction property between the metal and support material. It is known that the peaks corresponding to NiO species which have a weak metal–support interaction, nickel oxide species which have a strong interaction with alumina support, and nickel aluminate spinel appear in order of temperature increment [29]. When a Ni ion is incorporated into the alumina structure, stable nickel aluminate ($NiAl_2O_4$)-like species can be formed [19]. The Ni species in $NiAl_2O_4$ can be reduced to even higher temperature ranges [30]. Thus, it could be concluded that our Ni/Al_2O_3 have negligible Ni species of weakly interacted NiO-Al_2O_3, and mainly consist of strongly interacted NiO-Al_2O_3 and $NiAl_2O_4$.

Figure 2 exhibits the effects of the reaction temperature varying from 700 to 850 °C on CH_4 conversion, CO_2 conversion, H_2/CO ratio and H_2 selectivity, which were estimated by Equations (2)–(5).

$$CH_4 \text{ conversion } (\%) = (CH_{4\,in} - CH_{4\,out})/CH_{4\,in} \times 100 \quad (2)$$

$$CO_2 \text{ conversion } (\%) = (CO_{2\,in} - CO_{2\,out})/CO_{2\,in} \times 100 \quad (3)$$

$$H_2/CO = H_{2\,out}/CO_{\,out} \quad (4)$$

$$H_2 \text{ selectivity } (\%) = H_{2\,out}/2(CH_{4\,in} - CH_{4\,out}) \times 100 \quad (5)$$

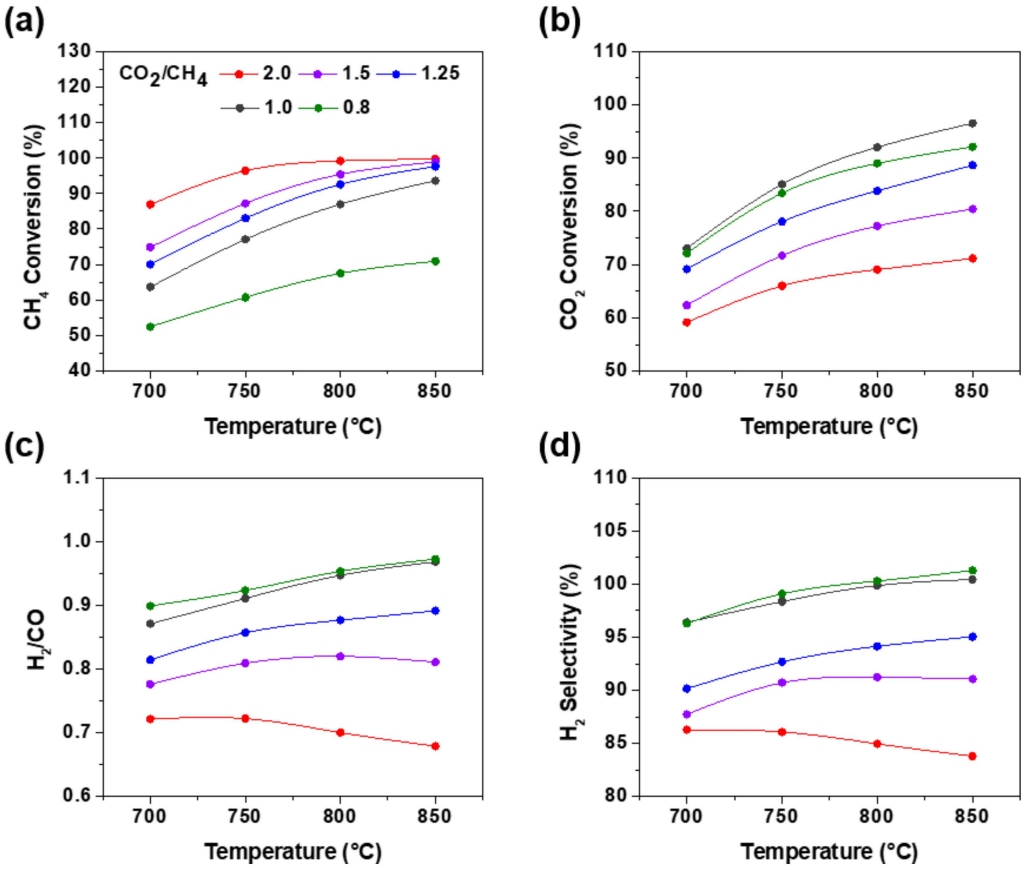

Figure 2. Influences of reaction temperature (700, 750, 800 and 850 °C) on (**a**) CH_4 conversion, (**b**) CO_2 conversion, (**c**) H_2/CO, (**d**) H_2 selectivity; N_2 = 20 mL·min^{-1}, WHSV = 60 L/g·h^{-1}.

As the reaction temperature increased, the conversions of both CO_2 and CH_4 rose, which is in line with the endothermic characteristics of a dry-reforming reaction. As the CO_2/CH_4 feed ratio increased, CH_4 conversion also increased; however, CO_2 conversion decreased except CO_2/CH_4 = 0.8 (Figure 2a,b). DRM is a reaction that consumes an equal amount of CO_2 and CH_4. As the ratio of CO_2/CH_4 rose, the amount of CO_2 that does not participate in DRM reaction increased. Therefore, CO_2 conversion decreased in order of CO_2/CH_4 = 1.0 > 1.25 > 1.5 > 2.0. Furthermore, the CH_4-rich condition led to a significant carbon deposition, which resulted in a reduction in the Ni active site; consequently, the opportunity of the CO_2 conversion decreased. Therefore, CO_2 conversion at CO_2/CH_4 = 0.8 was lower than CO_2/CH_4 = 1.0. As a result, CO_2 conversion at CO_2/CH_4 = 1.0 was the highest compared to other feed compositions. Chein et al. claimed that CO_2 takes a similar role to an oxidation agent in the combustion reaction. Thus, the more CO_2 in the feed gas, the more advantageous the reaction environment, resulting in the CH_4 conversion increasing in dry reforming [31]. Das et al. suggested the reaction mechanisms for the dry-reforming reaction, which involve the dissociative adsorption of CH_4 to form H_2 and CH_x intermediates, followed by the dissociation of adsorbed CO_2 on the Ni surface to form CO and Ni-O species. Subsequently, Ni-O and Ni-C react to form CO [32]. However, an insufficient amount of CO_2 (e.g., CO_2/CH_4 = 0.8) can lead to a deficiency of Ni-O, which

is necessary for the reaction with Ni-C to produce CO. In terms of CO_2 conversion, when the CO_2/CH_4 ratio is greater than 1, it is an excess amount, and CO_2 conversion seems to decrease, since in the study, it was sufficiently used in the drying reforming reaction and surplus CO_2 remained. The highest CO_2 conversion at all temperatures was observed when $CO_2/CH_4 = 1$ is used. As the amount of CO_2 exceeds CH_4, the H_2/CO ratio decreases due to the reverse water gas shift (RWGS) reaction (Equation (6)), which consumes hydrogen gas produced from DRM.

$$H_2 + CO_2 \rightarrow H_2O + 2CO \cdots \Delta H_{298K} = 41 \text{ kJ·mol}^{-1} \quad (6)$$

In addition, RWGS easily occurs when the flow rate of CO_2 is greater than that of CH_4. As a product of the RWGS reaction, we can visually confirm that water is produced and condensed at the end of the reactor. Serrano et al. experimentally showed that the increased CO_2/CH_4 ratio drove up the proportion of H_2O and reduced the H_2/CO ratio in the product gas [33]. When either $CO_2/CH_4 = 1$ or $CO_2/CH_4 = 0.8$ is used, the H_2/CO ratio and H_2 selectivity are significantly higher than those of other runs. This suggests that the dry-reforming reaction preferentially occurs in these cases rather than other side reactions, such as RWGS. With the exception of $CO_2/CH_4 = 2.0$, the H_2/CO ratio and H_2 selectivity increased as temperature increased, which is ascribed to the increment of hydrogen production attributed to the dry reforming of methane. However, when $CO_2/CH_4 = 2.0$, the H_2/CO ratio and H_2 selectivity decrease with the increasing temperature from 700 to 850 °C, suggesting that hydrogen consumption via the RWGS reaction is greater than hydrogen production from DRM as the reaction temperature rises.

Figure 3 shows the effects of space velocity varying from 60 to 240 $L/g{\cdot}h^{-1}$ on CH_4 conversion, CO_2 conversion, H_2/CO ratio, and H_2 selectivity. As the WHSV increased, the conversion of CO_2 and CH_4 significantly decreased. The higher WHSV means a shorter residence time of reactants with a catalyst bed, resulting in the conversion of CO_2 and CH_4 being decreased. For the case of $CO_2/CH_4 = 0.8$, conversion values dramatically decreased when WHSV is increased from 120 to 240 $L/g{\cdot}h^{-1}$, compared to other cases (Figure 3a,b). This indicates that a significant deactivation occurred due to a significant carbon deposition, as discussed later. The CH_4 conversion and CO_2 conversion for the CO_2/CH_4 feed ratio are a similar trend of the effect of a reaction temperature change, as shown in Figure 2. As shown in Figure 3a,b, the H_2/CO ratio and H_2 selectivity slightly decreased as WHSV increased, except for the $CO_2/CH_4 = 0.8$ run. For the case of $CO_2/CH_4 = 0.8$, the significant deactivation from 120 to 240 $L/g{\cdot}h^{-1}$ was observed due to a significant carbon deposition, as discussed later. Based on the carbon balance, we attempted to calculate the theoretical amount of carbon formation by employing Equations (7)–(9). The tendency of the carbon deposition amount relative to the feed ratio was consistent with the theoretical carbon formation.

$$\text{Carbon formation} = (C_{\text{in}} - C_{\text{out}}) \quad (7)$$

$$C_{\text{in}} = CH_{4\,\text{in}} + CO_{2\,\text{in}} \quad (8)$$

$$C_{\text{out}} = CH_{4\,\text{out}} + CO_{2\,\text{out}} + CO_{\text{out}} \quad (9)$$

$$C + CO_2 \rightarrow 2CO \cdots \Delta H_{298K} = 41 \text{ kJ·mol}^{-1} \quad (10)$$

$$CO_{\text{out}}/CO_{\text{DRM}} = CO_{\text{out}}/2(CH_{4\,\text{in}} - CH_{4\,\text{out}}) \quad (11)$$

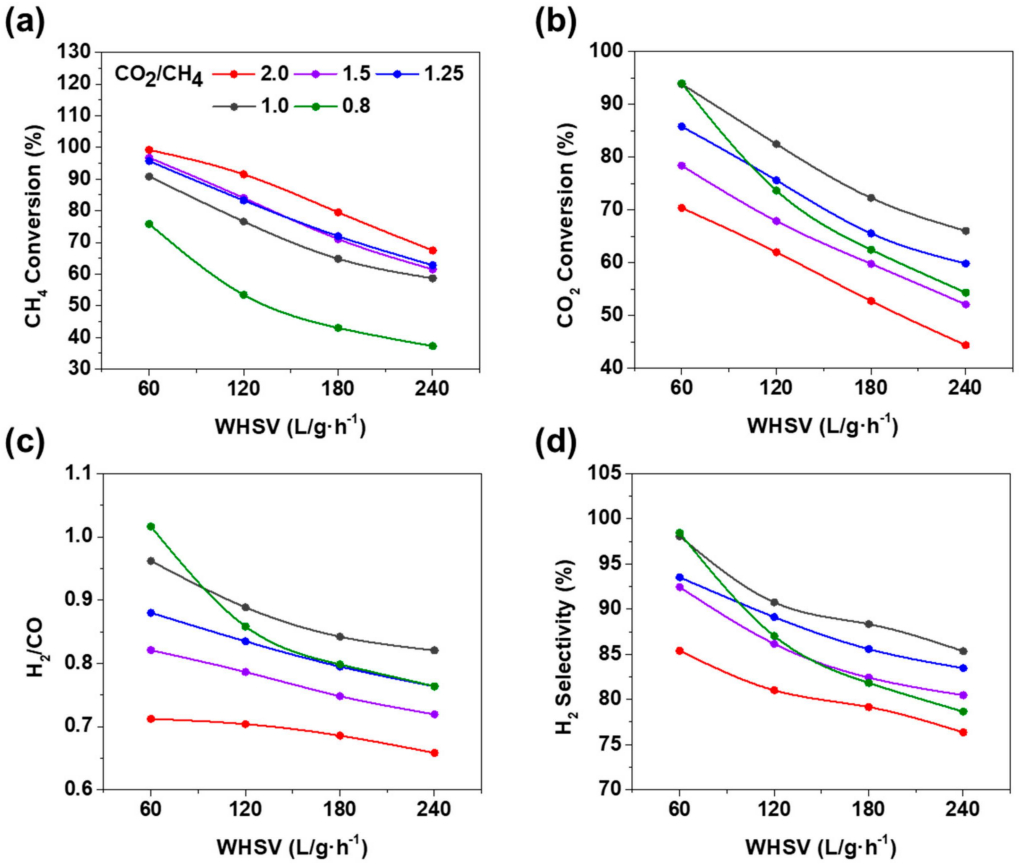

Figure 3. Influences of space velocity (60,120,180 and 240 L/g·h^{-1}) on (**a**) the CH_4 conversion, (**b**) CO_2 conversion, (**c**) H_2/CO, (**d**) H_2 selectivity; T = 800 °C, N_2 = 40 % *v*/*v* of total flow.

To estimate the catalytic activity of the Ni/Al_2O_3 catalyst in this work, we carried out stability tests at WHSV = 60 L/g·h^{-1}, CH_4:CO_2:N_2 = 3:3:4 and T = 850 °C. For 38 h of continuous DRM reactions, the CH_4 conversion (ca. 93%) and CO_2 conversion (ca. 96%) were well maintained; this should be expected to retain the catalytic activity for a longer period (Figure S2). We also operated a cyclic test for the Ni/Al_2O_3 catalyst at different WHSV of 60, 120, 180 L/g·h^{-1}, CH_4:CO_2:N_2 = 3:3:4 and T = 800 °C. The CH_4 conversion at each space velocity was 84%, 70% and 65%, respectively. The ratio of H_2/CO was 0.93, 0.87 and 0.82 in order of increased space velocity. In addition, this indicates that the CH_4 conversion, CO_2 conversion and ratio of H_2/CO were almost recovered with minor changes. This means that the stability and durability of Ni/Al_2O_3 catalyst is well maintained during severe reaction condition changes (Figure S3). Compared to the other previous research that applied the Ni/Al_2O_3 catalyst for DRM, we obtained reliable experimental results, and the Ni/Al_2O_3 catalyst in this study showed a reasonably stable catalytic performance (Table S1).

To evaluate the stability and durability of Ni catalysts in the DRM system, we conducted long-term activity tests at 850 °C for 600 min with different feed ratios (Figure 4). As shown in Figure 4a, for CO_2/CH_4 = 1.0 and 1.2, there was no significant deactivation until 10 h and the CH_4 conversions of 96 and 98% were maintained, respectively. In the case of CO_2/CH_4 = 0.8, the catalytic activity severely decreased until 120 min from the beginning of the dry-reforming reaction, and CH_4 conversion dropped from 80 to 73% at 30 min and 120 min, respectively (Figure 4a). After 120 min, the catalytic activity became quite stable, which can be ascribed to a reverse Boudouard reaction (Equation (10)). Based on the calculation of carbon balance and H_2/CO ratio, it should be assumed that a significant amount of carbon was formed at the beginning of the reaction due to the decomposition reaction of excess carbon (Excess $CH_4 \rightarrow C + 2H_2$). As the carbon deposition led to deacti-

vation, the conversion of CH_4 and CO_2 dropped drastically within 60 min. Although the carbon deposited on the Ni surface can hamper the DRM activity, it could be also used as a reactant on the reverse Boudouard reaction (Equation (10)), which made the aspect of deactivation quite stable [17]. As both the DRM reaction and reverse Boudouard reaction subsequently occurred, the catalytic activity can be quite elongated and become stable compared to that of the beginning. To understand the effect of side reactions, the amount of CO that can be produced by DRM was estimated by Equation (11) and was compared with the actual CO production, which were denoted as CO_{DRM} and CO_{out}, respectively (Figure S1b). In case of R0.8 conditions (CO_2/CH_4 = 0.8), CO_{out} was larger than CO_{DRM}, which indicates the occurrence of side reactions which can generate additional CO. The side reactions that produce CO should be the reverse water gas shift (RWGS) reaction and the reverse Boudouard reaction. Since the RWGS reaction consumes hydrogen produced from DRM, the H_2 selectivity can be significantly decreased if it is the main side reaction. When we compared hydrogen selectivity at R0.8 (CO_2/CH_4 = 0.8) and R1.0 (CO_2/CH_4 = 1.0), both cases showed similar selectivity ca. 98% (Figure S1a). It should be concluded that the catalyst drastically deactivated at the beginning due to a significant carbon formation and deposition; subsequently, the reverse Boudouard reaction decelerated the degradation in the CH_4-rich conditions. Regarding CO_2/CH_4 = 1.2, the H_2/CO ratio was relatively lower than CO_2/CH_4 = 1.0 and 0.8 (Figure 4b). The H_2/CO ratios of CO_2/CH_4 = 1.2, 1.0 and 0.8 were 0.90, 0.97 and 0.96, respectively. Excessive CO_2 is attributed to H_2 consumption due to the reverse water gas shift reaction (RWGS). Based on the above results, it is clear that insufficient CO_2 (CO_2/CH_4 = 0.8) induces significant coking, resulting in low performance in terms of both conversion and H_2 production. While the CO_2-rich condition (CO_2/CH_4 = 1.2) is slightly better in terms of conversion, it induces a significant RWGS reaction, resulting in a low H_2/CO ratio and H_2 selectivity. Therefore, we concluded that stoichiometric ratio (CO_2/CH_4 = 1.0) conditions are most beneficial for the DRM reaction.

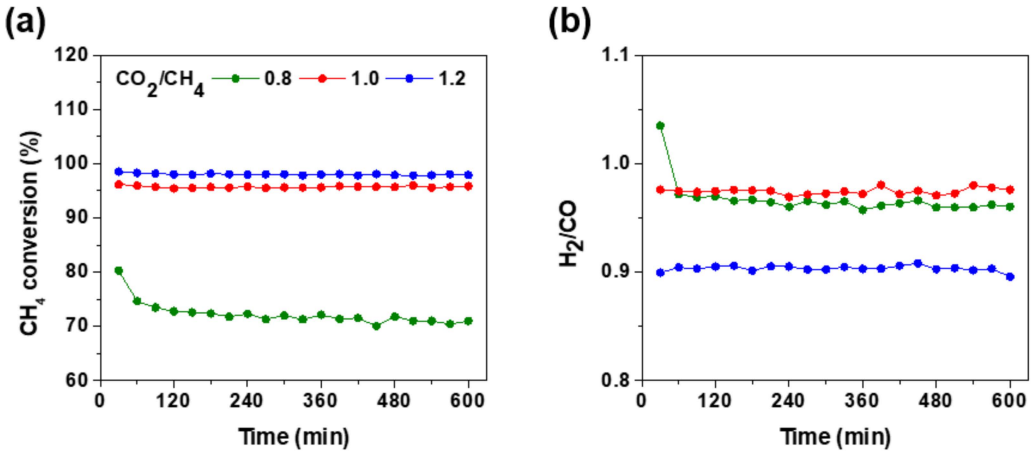

Figure 4. Time on stream results of the dry-reforming reaction with Ni/Al_2O_3 catalyst: (**a**) CH_4 conversion, (**b**) H_2/CO ratio; T = 850 °C, WHSV = 60 L/g·h^{-1}.

The Ni/Al_2O_3 catalysts after the DRM reaction were also characterized. As shown in Figure 5a, the Ni/Al_2O_3 catalyst showed well-maintained Ni peaks at 2θ = 44.3, 51.7 and 76.2°, and no NiO peak was observed after the dry-reforming reaction for 10 h. This indicates that nickel particles did not oxidize to NiO during the dry-reforming reaction. In addition, the Ni/Al_2O_3 catalyst after the DRM reaction showed a significant carbon (ICDD PDF 00-026-1076) peak at 2θ = 25.8° compared to the reduced catalyst before the reaction. We also evaluated the particle size of Ni after the DRM reaction. As shown in the XRD results, the Ni/Al_2O_3 catalyst after DRM showed a sharper Ni peak than the one before the reaction. The Ni particle size, which was calculated by the Scherrer formula, was changed from 10 nm to 16 nm after the DRM reaction. This implies the aggregation of Ni particles due to exposure to high temperatures during the DRM process [24], and can be

also confirmed by TEM analysis. As shown in Figure 5b, it can be easily seen that a Ni particle is sintered to a large particle (ca. ~17 nm) after the DRM reaction.

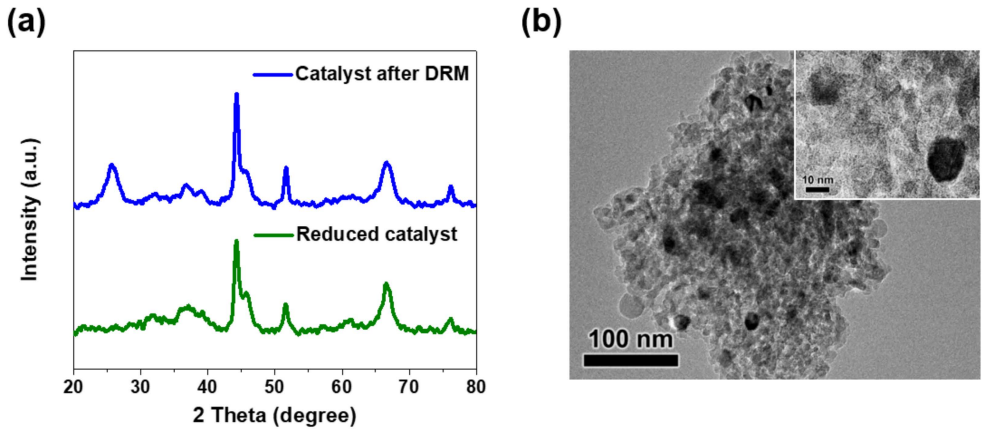

Figure 5. (**a**) X-ray diffraction (XRD) patterns of the reduced catalyst and the catalyst after DRM, (**b**) Transmission Electron Microscopy (TEM) images of the catalyst after DRM.

Figure 6 shows TGA profiles of the used catalysts after 10 h of the DRM reaction with different feed ratios (CO_2/CH_4 = 0.8, 1.0 and 1.2). The used catalysts were denoted as R0.8, R1.0 and R1.2, respectively, according to their feed ratio. It is widely acknowledged that weight loss at temperatures between 20 and 300 °C is a result of moisture being removed from the samples [34,35]. The amount of weight loss follows this order in this range: (R0.8 $\leq$ R1.0 $\leq$ R1.2). The moisture on the catalyst could correspond to water generated from the RWGS reaction during DRM. The consumption of hydrogen from DRM increased as the CO_2/CH_4 ratio became larger, which is consistent with the TGA results. The weight increase in the range of 300–400 °C is related to the oxidation of Ni to NiO on the surface of the catalyst [36]. All the catalysts showed weight increases due to Ni oxidation in this range, even though the increasing degree is slightly different. Finally, the significant weight loss is observed above 400 °C, which is ascribed to the oxidation of the coke on the catalyst surface [36,37]. Among the three catalysts, R0.8 exhibited a dramatic weight loss between 400 and 650 °C, and then a slight weight increase until 800 °C due to Ni oxidation after completely burning out the coke. The R1.0 sample exhibited a sharp decrease from 500 to 650 °C and a slight weight increase after 650 °C (Figure 6 inset), which is ascribed to the oxidation of Ni after the removal of carbon that has covered the surface of Ni during the DRM reaction. The R1.2 sample also showed similar behavior to R1.0. The weight loss from burning coke followed in order of R1.2(0.5%) < R1.0(2.6%) < R0.8(28.1%). A significant amount of filamentous carbon on the surface of the catalyst was observed in the TEM images of R0.8 (Figure 6b).

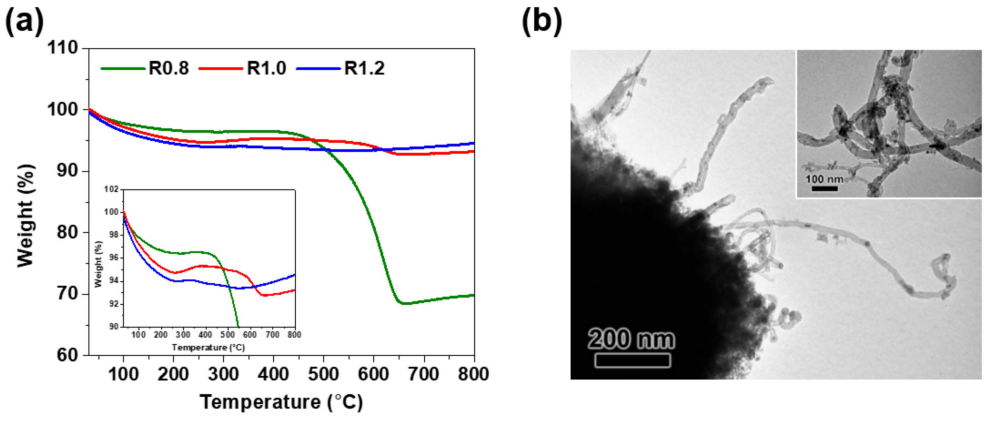

Figure 6. (**a**) TGA profiles of the spent catalysts after 10 h of DRM reaction, (**b**) Transmission Electron Microscopy (TEM) images of the spent catalyst after 10 h of dry reforming (R0.8).

We also analyzed the structures of carbon deposited on the catalysts. Figure 7 displays the Raman spectra of two catalysts (R0.8 and R1.0) which exhibited obvious TGA weight loss above 500 °C after a 10 h DRM reaction. Corresponding to the TGA analysis, there was no significant peak in the Raman spectra of R1.2 due to the negligible amount of carbon deposited on R1.2. Both R0.8 and R1.0 showed two obvious vibration bands: the D-band (1350 cm^{-1}) and the G-band (1580 cm^{-1}), which are typical characteristics of carbon materials. The Raman spectrum intensity of R0.8 was higher than that of R1.0, indicating that R0.8 has a large number of carbon species on the surface compared to R1.0. It is known that the D band is related to the presence of defects or a disordered carbon structure, and the G band is attributed to the C = C stretching vibration of sp^2 carbon [38,39]. Generally, the intensity ratio of the D band and G band (I_D/I_G) is an indicator of the graphitic degree of carbon; the lower the value, the more graphitic the structure [40,41]. For R0.8 and R1.0, the respective I_D/I_G values are 0.919 and 0.751, indicating that the graphitic degree becomes lower as the R-value increases. Therefore, the carbon deposited on R0.8 has as less graphitic properties as that on R1.0 [42]. Although the absolute amount of carbon deposited on R0.8 is much larger than that of R1.0, as a result of the more defective structure of the coke deposited on R0.8 than R1.0, the carbon on R1.0 oxidized at a higher temperature than R0.8. This is consistent with the TGA results—weight loss by the carbon oxidation of R0.8 started at 450 °C, while weight loss by coke burning of R1.0 started at 550 °C. Charisiou et al. reported that the combustion temperature varies depending on the species of carbon [25]. The temperature increases in the order of amorphous carbon, carbon allotropes with defects in the graphitic lattice and highly graphitized carbon nanotubes. Guo et al. similarly observed that two types of carbon, amorphous and graphitic-like carbon, deposited on the Ni catalyst after methane decomposition. Graphitic-like carbon fully oxidized at higher temperatures than amorphous carbon [43].

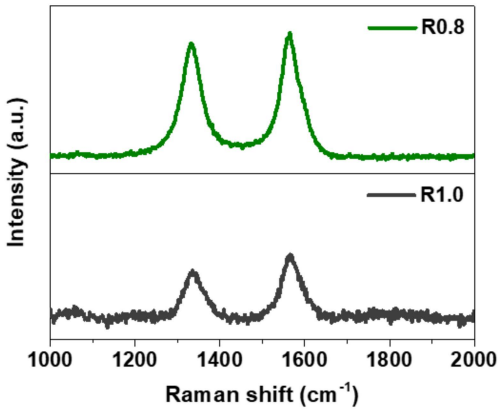

Figure 7. The Raman spectra of spent catalysts after 10 h of DRM reactions.

3. Materials and Methods

3.1. Materials

Commercial alumina spheres (particle diameter = 2.5 mm, specific surface area = 200–220 m^2/g) were provided by Sasol (Johannesburg, Republic of South Africa). The alumina ball was crushed to a powder using a mortar and pestle and sieved to the particle size range of 100–150 μm. Nickel nitrate hexahydrate ($Ni(NO_3)_2{\cdot}6H_2O$) was purchased from Daejung (Siheung, Republic of Korea).

3.2. Synthesis

A Ni/Al_2O_3 catalyst was prepared using the conventional wet impregnation method. The necessary amount of $Ni(NO_3)_2{\cdot}6H_2O$ was dissolved in distilled water and used to impregnate the alumina support. After drying in a rotary evaporator at 80 °C, the sample was calcined at 700 °C for 3 h with a ramping rate of 4.25 °C/min. Finally, the catalysts

were sieved to a particle size of 100–150 microns and used for additional characterization and reaction tests.

3.3. Characterization

X-ray diffraction analysis (XRD) was conducted using D/MAX 2200 (Rigaku, Tokyo, Japan, Cu Kα, λ = 1.5418 Å). The scanning range was from 20 to 80° and the scanning speed was 8°/min. Textural properties were characterized using Tristar II 3020 (Micromeritics, Norcross, USA) through N_2 adsorption–desorption at 77 K. The temperature-programmed reduction (H_2-TPR) was performed using BELCAT-M (MicrotracBEL, Osaka, Japan). The pre-treated catalyst was heated from 30 to 1000 °C with a ramping rate of 5 °C/min, under H_2 balanced with Ar gas conditions (5%, 30 mL/min). The amount of coke formation was then evaluated using a thermal gravimetric analyzer, TGA N-1000 (Scinco, Seoul, Republic of Korea). The samples were heated from 30 to 800 °C at a ramping rate of 5 °C/min in an air atmosphere. The coke-on catalyst after the dry-reforming reaction was analyzed by Raman spectroscopy, SR-303i (Andor Technology, Belfast, Northern Ireland) with a 532 nm laser module.

3.4. Catalytic Activity Test (Dry Reforming of Methane)

Catalytic activity tests of the Ni/Al_2O_3 catalyst were carried out in a continuous flow fixed-bed quartz reactor. Catalysts (50 mg) were placed in a reactor bed (ID = 3/8″) between quartz wool beds. A K-type thermocouple was used to monitor the reaction temperature, and a mass flow controller was used to precisely control the flow rates of nitrogen, methane and carbon dioxide (N_2, CH_4 and CO_2).

Prior to the dry-reforming reaction, the temperature was raised to 800 °C with N_2 flow, and the catalyst was reduced to 800 °C under 20 mL/min flow of pure H_2 for 1 h. To investigate the effect of temperature, the reaction experiment was conducted at 700, 750, 800 and 850 °C for 1 h, respectively. Temperature was controlled using a stepwise mode of the PID controller, and the reaction was conducted for 1 h in each temperature once it was stabilized. In addition, the reaction experiments were operated with varying feed compositions while the WHSV was adjusted to 60 $L{\cdot}g^{-1}h^{-1}$, and the N_2 flow rate was fixed at 20 mL/min. To investigate the effect of space velocity, a reaction experiment was conducted at a constant temperature of 800 °C with four different WHSV values of 60, 120, 180 and 240 $L{\cdot}g^{-1}h^{-1}$. Each of these space velocities was maintained for 1 h once stabilized. Additionally, the reaction experiment was conducted with various CO_2/CH_4 feed ratios of 0.8, 1.0 and 1.2, and was run for a long-term period. After reducing the catalyst at 800 °C for 90 min with an H_2:N_2 ratio of 1:1 under a constant flow of 40 mL/min, catalytic activity tests were conducted at 850 °C for 10 h.

The reaction effluent gases from the DRM reactor were analyzed by online gas chromatography, YL-6500 (Young In Chromass, Anyang, Republic of Korea) equipped with a thermal conductivity detector and Carboxen-1000 (Supelco Analytical, Bellefonte, PA, USA) as a GC column. Ar was employed as the carrier gas for quantifying the H_2, N_2, CO, CH_4 and CO_2 in the product gas. N_2 was utilized as an internal standard, and the component of gas after the dry-reforming reaction was calculated based on N_2.

4. Conclusions

We synthesized a conventional Ni/Al_2O_3 catalyst and applied it to a dry-reforming reaction. We investigated the effect of operating parameters such as reaction temperature, space velocity and feed composition on the overall performance of the dry-reforming reaction of methane over the Ni/Al_2O_3 catalyst. As the reaction temperature elevated, the dry-reforming reaction, which has endothermic property, was accelerated; consequently, the methane conversion increased. Furthermore, the CH_4 conversion declined as the space velocity increased due to the decrement in residence time, which led to a lack of opportunity that both reactant gas and the catalyst surface can contact. The conversion of methane increased as the ratio of carbon dioxide in the feed gas became higher. However, the

excessive carbon dioxide in the feed gas promoted the reverse water gas shift reaction, which consumed the produced hydrogen, resulting in a low H_2/CO ratio and H_2 selectivity. The composition of reactant gas was significantly related to the side reactions during the DRM reaction. Indeed, excessive methane in the feed gas significantly caused the carbon formation, consequently dramatically decreasing the catalytic activity due to the coke covering the active site of Ni. In addition, the quantity and quality of carbon deposited on the catalyst after a reaction depends heavily on the CO_2-to-CH_4 ratio in the feed gas. When excessive CO_2 (R1.2) was involved in the DRM reaction, only an insignificant amount of carbon was deposited on the catalyst. Furthermore, a strict adherence to stoichiometric conditions (R1.0) gave rise to carbon species that burn off at high temperatures; however, when the feed gas was CH_4-rich (R0.8), a larger amount of coke was created, leading to a considerable decrease in catalyst performance. Our results indicated that the feed gas composition is a major factor in determining the performance of Ni-based catalysts in DRM. We, therefore, suggest that the optimal gas conditions to achieve the highest conversion, hydrogen production and long-term stability are in the range of the stoichiometric conditions.

Supplementary Materials: The following supporting information can be downloaded at: https://www.mdpi.com/article/10.3390/catal13030602/s1, Figure S1: Time on stream results of dry reforming reaction with Ni/Al_2O_3 catalyst: (a) H_2 selectivity, (b) COout/CODRM ratio; T = 850 °C, WHSV = 60 $L/g{\cdot}h^{-1}$.; Figure S2: Time on stream results of dry reforming reaction over Ni/Al_2O_3 catalyst; T = 850 °C, WHSV = 60 $L/g{\cdot}h^{-1}$, CH_4:CO_2:N_2 = 3:3:4.; Figure S3: Time on stream results of dry reforming reaction over Ni/Al_2O_3 catalyst with different WHSV of 60, 120, 180 $L/g{\cdot}h^{-1}$: (a) Conversion of CH_4 and CO_2, (b) H_2/CO ratio; T = 800 °C, CH_4:CO_2:N_2 = 3:3:4.; Table S1: Comparative research on dry reforming of methane over Ni/Al_2O_3 catalyst [19,29,44].

Author Contributions: Investigation and writing—original draft preparation, E.Y.; Methodology, D.-S.C.; Analysis, J.K.; Visualization, Y.-H.K.; Resources, N.-Y.K.; Conceptualization, Writing—review and editing, and supervision, J.B.J. All authors have read and agreed to the published version of the manuscript.

Funding: This research was supported by the National Research Foundation of Korea (NRF) grant funded by the Korean government's Ministry of Science and ICT (MSIT) (NRF-2022M3J2A1085554). This work is also supported by the Waste to Energy-Recycling Human Resource Development Project (YL-WE-21-001).

Conflicts of Interest: The authors declare no conflict of interest.

References

1. Wadanambi, R.T.; Wandana, L.S.; Chathumini, K.K.G.L.; Dassanayake, N.P.; Preethika, D.D.P.; Arachchige, U.S.P.R. The effects of industrialization on climate change. *J. Res. Technol. Eng.* **2020**, *1*, 86–94.
2. Perera, F. Pollution from fossil-fuel combustion is the leading environmental threat to global pediatric health and equity: Solutions exist. *Int. J. Environ. Res. Public Health* **2018**, *15*, 16. [CrossRef] [PubMed]
3. Chu, S.; Cui, Y.; Liu, N. The path towards sustainable energy. *Nat. Mater.* **2017**, *16*, 16–22. [CrossRef]
4. Latha, K.; Velraj, R.; Shanmugam, P.; Sivanesan, S. Mixing strategies of high solids anaerobic co-digestion using food waste with sewage sludge for enhanced biogas production. *J. Clean. Prod.* **2019**, *210*, 388–400. [CrossRef]
5. Maragkaki, A.; Vasileiadis, I.; Fountoulakis, M.; Kyriakou, A.; Lasaridi, K.; Manios, T. Improving biogas production from anaerobic co-digestion of sewage sludge with a thermal dried mixture of food waste, cheese whey and olive mill wastewater. *Waste Manag.* **2018**, *71*, 644–651. [CrossRef] [PubMed]
6. Kim, M.; Li, D.; Choi, O.; Sang, B.-I.; Chiang, P.C.; Kim, H. Effects of supplement additives on anaerobic biogas production. *Korean J. Chem. Eng.* **2017**, *34*, 2678–2685. [CrossRef]
7. Augelletti, R.; Conti, M.; Annesini, M.C. Pressure swing adsorption for biogas upgrading. A new process configuration for the separation of biomethane and carbon dioxide. *J. Clean. Prod.* **2017**, *140*, 1390–1398. [CrossRef]
8. Vrbová, V.; Ciahotný, K. Upgrading biogas to biomethane using membrane separation. *Energy Fuels* **2017**, *31*, 9393–9401. [CrossRef]
9. Sarafraz, M.; Christo, F.; Safaei, M.R. Potential of plasmonic microreactor for Photothermal hydrogen-enriched fuel production from biomethane. *Int. J. Hydrogen Energy* **2022**, *47*, 26355–26368. [CrossRef]

10. Jayaram, V.; Arun, J.; Jacob, N.B.B.; Abraham, V.V.G. Enrichment of calorific value for low pressure biogas. *Int. J. Adv. Sci. Technol.* **2017**, *3*, 199–201.
11. Lim, Y.-K.; Lee, J.-M.; Jung, C.-S. The status of biogas as renewable energy. *Appl. Chem. Eng.* **2012**, *23*, 125–130.
12. Lang, C.; Sécordel, X.; Kiennemann, A.; Courson, C. Water gas shift catalysts for hydrogen production from biomass steam gasification. *Fuel Process. Technol.* **2017**, *156*, 246–252. [CrossRef]
13. Kalai, D.Y.; Stangeland, K.; Jin, Y.; Tucho, W.M.; Yu, Z. Biogas dry reforming for syngas production on La promoted hydrotalcite-derived Ni catalysts. *Int. J. Hydrogen Energy* **2018**, *43*, 19438–19450. [CrossRef]
14. Hamzehlouia, S.; Jaffer, S.A.; Chaouki, J. Microwave Heating-Assisted Catalytic Dry Reforming of Methane to Syngas. *Sci. Rep.* **2018**, *8*, 8940. [CrossRef] [PubMed]
15. Sonal; Ahmad, E.; Upadhyayula, S.; Pant, K.K. Biomass-derived CO_2 rich syngas conversion to higher hydrocarbon via Fischer-Tropsch process over Fe-Co bimetallic catalyst. *Int. J. Hydrogen Energy* **2019**, *44*, 27741–27748. [CrossRef]
16. Song, H.; Jung, H.S.; Uhm, S. Recent progress for hydrogen production from biogas and its effective applications. *Appl. Chem. Eng.* **2020**, *31*, 1–6.
17. Omoregbe, O.; Danh, H.T.; Nguyen-Huy, C.; Setiabudi, H.; Abidin, S.; Truong, Q.D.; Vo, D.-V.N. Syngas production from methane dry reforming over Ni/SBA-15 catalyst: Effect of operating parameters. *Int. J. Hydrogen Energy* **2017**, *42*, 11283–11294. [CrossRef]
18. Dai, Y.-M.; Lu, C.-Y.; Chang, C.-J. Catalytic activity of mesoporous Ni/CNT, Ni/SBA-15 and (Cu, Ca, Mg, Mn, Co)–Ni/SBA-15 catalysts for CO_2 reforming of CH_4. *RSC Adv.* **2016**, *6*, 73887–73896. [CrossRef]
19. Bian, Z.; Zhong, W.; Yu, Y.; Wang, Z.; Jiang, B.; Kawi, S. Dry reforming of methane on Ni/mesoporous-Al_2O_3 catalysts: Effect of calcination temperature. *Int. J. Hydrogen Energy* **2021**, *46*, 31041–31053. [CrossRef]
20. Gholizadeh, F.; Izadbakhsh, A.; Huang, J.; Zi-Feng, Y. Catalytic performance of cubic ordered mesoporous alumina supported nickel catalysts in dry reforming of methane. *Microporous Mesoporous Mater.* **2021**, *310*, 110616. [CrossRef]
21. Han, J.W.; Park, J.S.; Choi, M.S.; Lee, H. Uncoupling the size and support effects of Ni catalysts for dry reforming of methane. *Appl. Catal. B Environ.* **2017**, *203*, 625–632. [CrossRef]
22. Tao, M.; Xin, Z.; Meng, X.; Bian, Z.; Lv, Y. Highly dispersed nickel within mesochannels of SBA-15 for CO methanation with enhanced activity and excellent thermostability. *Fuel* **2017**, *188*, 267–276. [CrossRef]
23. Kim, J.-H.; Suh, D.J.; Park, T.-J.; Kim, K.-L. Effect of metal particle size on coking during CO_2 reforming of CH_4 over Ni-alumina aerogel catalysts. *Appl. Catal. A Gen.* **2000**, *197*, 191–200. [CrossRef]
24. Song, Y.; Ozdemir, E.; Ramesh, S.; Adishev, A.; Subramanian, S.; Harale, A.; Albuali, M.; Fadhel, B.A.; Jamal, A.; Moon, D.; et al. Dry reforming of methane by stable Ni-Mo nanocatalysts on single-crystalline MgO. *Science* **2020**, *367*, 777–781. [CrossRef] [PubMed]
25. Charisiou, N.D.; Douvartzides, S.L.; Siakavelas, G.I.; Tzounis, L.; Sebastian, V.; Stolojan, V.; Hinder, S.J.; Baker, M.A.; Polychronopoulou, K.; Goula, M.A. The relationship between reaction temperature and carbon deposition on nickel catalysts based on Al_2O_3, ZrO_2 or SiO_2 supports during the biogas dry reforming reaction. *Catalysts* **2019**, *9*, 676. [CrossRef]
26. Schwengber, C.A.; da Silva, F.A.; Schaffner, R.A.; Fernandes-Machado, N.R.C.; Ferracin, R.J.; Bach, V.R.; Alves, H.J. Methane dry reforming using Ni/Al_2O_3 catalysts: Evaluation of the effects of temperature, space velocity and reaction time. *J. Environ. Chem. Eng.* **2016**, *4*, 3688–3695. [CrossRef]
27. Gonçalves, A.A.S.; Costa, M.J.F.; Zhang, L.; Ciesielczyk, F.; Jaroniec, M. One-Pot Synthesis of $MeAl_2O_4$ (Me = Ni, Co, or Cu) Supported on γ-Al_2O_3 with Ultralarge Mesopores: Enhancing Interfacial Defects in γ-Al_2O_3 to Facilitate the Formation of Spinel Structures at Lower Temperatures. *Chem. Mater.* **2018**, *30*, 436–446. [CrossRef]
28. Yuan, Q.; Yin, A.-X.; Luo, C.; Sun, L.-D.; Zhang, Y.-W.; Duan, W.-T.; Liu, H.-C.; Yan, C.-H. Facile Synthesis for Ordered Mesoporous γ-Aluminas with High Thermal Stability. *J. Am. Chem. Soc.* **2008**, *130*, 3465–3472. [CrossRef]
29. He, L.; Ren, Y.; Yue, B.; Tsang, S.; He, H. Tuning Metal-Support Interactions on Ni/Al_2O_3 Catalysts to Improve Catalytic Activity and Stability for Dry Reforming of Methane. *Processes* **2021**, *9*, 706. [CrossRef]
30. Morales-Marín, A.; Ayastuy, J.; Iriarte-Velasco, U.; Gutiérrez-Ortiz, M. Nickel aluminate spinel-derived catalysts for the aqueous phase reforming of glycerol: Effect of reduction temperature. *Appl. Catal. B Environ.* **2018**, *244*, 931–945. [CrossRef]
31. Chein, R.; Yang, Z. Experimental Study on Dry Reforming of Biogas for Syngas Production over Ni-Based Catalysts. *ACS Omega* **2019**, *4*, 20911–20922. [CrossRef] [PubMed]
32. Das, S.; Ashok, J.; Bian, Z.; Dewangan, N.; Wai, M.; Du, Y.; Borgna, A.; Hidajat, K.; Kawi, S. Silica-Ceria sandwiched Ni core-shell catalyst for low temperature dry reforming of biogas: Coke resistance and mechanistic insights. *Appl. Catal. B Environ.* **2018**, *230*, 220–236. [CrossRef]
33. Serrano-Lotina, A.; Daza, L. Influence of the operating parameters over dry reforming of methane to syngas. *Int. J. Hydrogen Energy* **2014**, *39*, 4089–4094. [CrossRef]
34. Al-Najar, A.M.; Al-Doghachi, F.A.; Al-Riyahee, A.A.; Taufiq-Yap, Y.H. Effect of La_2O_3 as a promoter on the Pt, Pd, Ni/MgO catalyst in dry reforming of methane reaction. *Catalysts* **2020**, *10*, 750. [CrossRef]
35. Komarala, E.P.; Komissarov, I.; Rosen, B.A. Effect of Fe and Mn substitution in $LaNiO_3$ on exsolution, activity, and stability for methane dry reforming. *Catalysts* **2019**, *10*, 27. [CrossRef]
36. Shin, S.A.; Alizadeh Eslami, A.; Noh, Y.S.; Song, H.-t.; Kim, H.D.; Ghaffari Saeidabad, N.; Moon, D.J. Preparation and Characterization of Ni/ZrTiAlO x Catalyst via Sol-Gel and Impregnation Methods for Low Temperature Dry Reforming of Methane. *Catalysts* **2020**, *10*, 1335. [CrossRef]

37. Park, S.-W.; Lee, D.; Kim, S.-I.; Kim, Y.; Park, J.; Heo, I.; Chang, T.; Lee, J. Effects of Alkali Metals on Nickel/Alumina Catalyzed Ethanol Dry Reforming. *Catalysts* **2021**, *11*, 260. [CrossRef]
38. Sheka, E.F.; Golubev, Y.A.; Popova, N.A. Graphene domain signature of Raman spectra of sp 2 amorphous carbons. *Nanomaterials* **2020**, *10*, 2021. [CrossRef]
39. Liu, Y.; Xu, H.; Yu, H.; Yang, H.; Chen, T. Synthesis of lignin-derived nitrogen-doped carbon as a novel catalyst for 4-NP reduction evaluation. *Sci. Rep.* **2020**, *10*, 20075. [CrossRef]
40. Kassab, L.R.P.; Santos, A.D.d.; Pillis, M.F. Evaluation of carbon thin films using Raman spectroscopy. *Mater. Res.* **2018**, *21*, e20170787.
41. Alotaibi, N.; Hammud, H.H.; Al Otaibi, N.; Prakasam, T. Electrocatalytic properties of 3D hierarchical graphitic carbon-cobalt nanoparticles for urea oxidation. *ACS Omega* **2020**, *5*, 26038–26048. [CrossRef] [PubMed]
42. Akri, M.; El Kasmi, A.; Batiot-Dupeyrat, C.; Qiao, B. Highly Active and Carbon-Resistant Nickel Single-Atom Catalysts for Methane Dry Reforming. *Catalysts* **2020**, *10*, 630. [CrossRef]
43. Guo, J.; Lou, H.; Zheng, X. The deposition of coke from methane on a $Ni/MgAl_2O_4$ catalyst. *Carbon* **2007**, *45*, 1314–1321. [CrossRef]
44. Dekkar, S.; Tezkratt, S.; Sellam, D.; Ikkour, K.; Parkhomenko, K.; Martinez-Martin, A.; Roger, A.C. Dry Reforming of Methane over $Ni\text{-}Al_2O_3$ and $Ni\text{-}SiO_2$ Catalysts: Role of Preparation Methods. *Catal. Lett.* **2020**, *150*, 2180–2199. [CrossRef]